

## Brief papers

## Path planning for solar-powered UAV in urban environment

Jianfa Wu<sup>a,b,c</sup>, Honglun Wang<sup>a,c,\*</sup>, Na Li<sup>d</sup>, Peng Yao<sup>e</sup>, Yu Huang<sup>f</sup>, Hemeng Yang<sup>g</sup><sup>a</sup>School of Automation Science and Electrical Engineering, Beihang University, Beijing 100191, China<sup>b</sup>Shenyuan Honors College of Beihang University, Beijing 100191, China<sup>c</sup>Science and Technology on Aircraft Control Laboratory, Beihang University, Beijing 100191, China<sup>d</sup>Unmanned System Research Institute, Beihang University, Beijing 100191, China<sup>e</sup>College of Engineering, Ocean University of China, Qingdao 266100, China<sup>f</sup>Institute of Public Safety Research, Tsinghua University, Beijing 100084, China<sup>g</sup>Tianjin Zhongwei Aerospace Data System Technology Co., Ltd, Tianjin 300301, China

## ARTICLE INFO

## Article history:

Received 19 July 2017

Revised 11 October 2017

Accepted 20 October 2017

Available online 11 November 2017

## Keywords:

Urban environment

Solar-powered UAV (SUAV)

Path planning

Restrained Interfered Fluid Dynamical System (RIFDS)

Improved Whale Optimization Algorithm (IWOA)

ASHRAE Clear Sky Model

## ABSTRACT

Aiming at the complexity and particularity of urban environment, a solar-powered UAV (SUAV) path planning framework is proposed in this paper. The framework can be decomposed into three aspects to resolve. First, to make SUAV avoid the building obstacles, a nature-inspired path planning method called Interfered Fluid Dynamical System (IFDS) is introduced. Aiming at the defect that the traditional IFDS is not suitable for SUAV energy optimization calculation, the dynamic constraints and model are introduced to IFDS. The modified IFDS, called Restrained IFDS (RIFDS), is proposed. Second, to resolve the path planning issue efficiently, a novel intelligent optimization algorithm called Whale Optimization Algorithm (WOA) is selected as the basic framework solver. To further overcome the drawback of local minima, adaptive chaos-Gaussian switching solving strategy and coordinated decision-making mechanism are introduced to the basic WOA. The modified algorithm, called Improved WOA (IWOA), is proposed. Third, to solve the accurate modeling problem of solar energy in urban environment, two measures are adopted: (1) A practical judgment method for sunlight occlusions is proposed; (2) Aiming at some unreasonable aspects in the solar energy production model, the received solar energy is modified and recalculated by ASHRAE Clear Sky Model and the solar irradiance calculation principle for slant surfaces in this paper. Finally, the effectiveness of the proposed framework is tested by the simulations.

© 2017 Elsevier B.V. All rights reserved.

## 1. Introduction

With the boom of urbanization, the demand for small Unmanned Aerial Vehicles (UAVs) flying at low altitudes increases rapidly. The small UAV in city can execute the missions such as police patrols, news reports, high building fire control, etc. These missions have rigorous requirements for the endurance time. However, the traditional small UAV is limited by its load as it cannot reserve more energy and be qualified for the work. Solar-powered UAVs (SUAVs) utilize solar radiation as energy. Compared with the traditional UAV, SUAV has a better endurance performance. Hence, small SUAVs like those mentioned in [1,2] are suitable for long endurance missions in city. Currently, the corresponding SUAV technology has been widely focused on and studied, especially the aspects of energy optimization and management [3–5]. Because current studies on the energy exchange efficiencies of solar cells cannot make breakthroughs within a short time, optimizing flight

paths has become an effective methodology to make SUAV receive more solar radiation. Klesh and Kabamba [1] establish the energy harvesting and consumption model and design the energy-optimal path for SUAV. Dai et al. [6,7] extend the energy-optimal path from 2D space to 3D space. Hosseini et al. [8,9] plan the SUAV path for the area surveillance problem. Spangelo and Gilbert [2] plan the path of SUAV for ground target tracking. The aforementioned studies have achieved important results for SUAV path planning in free environment and have laid the foundation for SUAV path planning. However, in urban environment, these methods may not be suitable for the following reasons:

- (1) The high buildings in city will influence the flight safety as they are obstacles. However, the aforementioned studies only consider the energy optimization problem and focus on the path planning in free environment, but do not design a proper obstacle avoidance strategy.
- (2) High buildings may block out sunlight and generate “shadow regions”. The range of a shadow region depends on the height difference between SUAV and buildings and the solar angles. Hence, the range of a shadow region is time-variable.

\* Corresponding author at: School of Automation Science and Electrical Engineering, Beihang University, Beijing 100191, China.

If SUAV is located in a shadow region, the received solar radiation can be regarded as zero. Because the accurate modeling of urban environment is a precondition for SUAV energy-optimal path planning, the sunlight occlusions by buildings must be taken into consideration. However, it seems that there is no literature considering the sunlight occlusions for SUAV. This is the most distinct difference between urban and free environments for SUAV applications.

- (3) According to the research achievements of solar engineering [10,11], solar radiation can be divided into three parts: the beam component, the diffuse component, and the ground reflected component. However, in the aforementioned studies, only the beam radiation is considered and is simplified as a constant, i.e., an average value for SUAV. Actually, by [10,11], the values of the beam radiation and diffuse radiation can be calculated accurately according to the date. Moreover, because SUAV flies near the ground in city, the ground reflected solar radiation should be considered for the more accurate energy modeling.

Due to the complexity of urban environment caused by the coupling of obstacle avoidance and energy optimization, according to our present investigation, no related literature specializes in SUAV path planning in urban environment. Therefore, this paper focuses on solving this issue by decomposing it into the following aspects.

First, to solve the obstacle avoidance problem, a novel nature-inspired methodology called Interfered Fluid Dynamical System (IFDS), which is proposed in our previous work [12–14], is introduced. IFDS imitates the phenomenon through which water in river smoothly avoids rocks and eventually reaches the destination. Unlike other nature-inspired methodologies e.g., the method which directly optimizes a series of waypoints in the path via the intelligent algorithm [15–20], IFDS generates a smooth streamline (i.e., planned path) according to some parameters of each obstacle. The biggest advantage of IFDS is the smooth planned paths. However, IFDS from our previous work cannot be applied in SUAV path planning directly because of the following reasons:

- (1) SUAV needs to adjust its attitude (especially its direction and bank angles) to track the solar incidence direction in real time so that the cells on the surface of wings can obtain as much solar radiation as possible. Nevertheless, the streamline generated by IFDS is merely a series of UAV positions, which do not contain the attitude information directly. This defect may not influence the traditional UAV, but it is negligible for SUAV energy-optimal path planning.
- (2) For flight safety, some states of UAV are set as the restrained values according to the dynamic performances e.g., the bank angle is limited for the SUAV mentioned in [1]. However, in the traditional IFDS, the states of UAV are not restrained. Hence, the feasibility of the planned path cannot be guaranteed.

In general, the biggest defect of the traditional IFDS is that it is divorced from the UAV dynamic model. Therefore, we will introduce the UAV model and constraints for IFDS. The modified IFDS proposed in this paper for SUAV is called Restrained IFDS (RIFDS).

Second, to resolve the optimal paths, an efficient solver is introduced. This solver, unlike the traditional mathematical programming methods such as the mixed integer linear programming, nonlinear programming, etc., uses intelligent optimization algorithms (IOAs) to effectively avoid the problem of “combination blast”. IOAs imitate natural phenomena to search the optimal solution efficiently. Currently, the traditional IOAs applied in UAV path planning include Genetic Algorithm (GA) [20], Particle Swarm Optimization (PSO) [21], Differential Evolution (DE) [22], Gravitational Search Algorithm (GSA) [23], Pigeon-inspired Optimization (PIO)

[16], Artificial Bee Colony (ABC) [18], Grey Wolf Optimizer (GWO) [24], Backtracking Search Algorithm (BSA) [25], etc. In recent years, a novel swarm-based optimization algorithm called Whale Optimization Algorithm (WOA) is proposed by Mirjalili, which imitates the hunting behavior of humpback whales [26]. According to the theoretical analysis and many numerical experiments, compared with the traditional IOAs, WOA has a faster solution speed and a higher accuracy. Hence, we would like to select WOA as the solver for our problem. However, the original WOA still has the drawback that it may become trapped in local minima. To overcome this drawback, some improvements are proposed and introduced to WOA in this paper. The modified WOA is called Improved WOA (IWOA).

Third, to solve the accurate modeling problem of solar energy in urban environment, two measures are adopted in this paper: First, a practical judgement method for the shadow region is proposed. Second, SUAV is regarded as a piece of flying solar panel so that the received energy can be recalculated by the knowledge in the field of the solar engineering, i.e., ASHRAE (American Society of Heating, Refrigerating and Air-conditioning Engineers) Clear Sky Model [11].

The contributions of this paper can be summarized as follows:

- (1) An SUAV path planning framework aimed at urban environment is proposed. The obstacle condition and the shadow regions caused by high buildings are considered.
- (2) Dynamic constraints and model are introduced to the traditional IFDS. The modified IFDS, called RIFDS, is proposed. The necessary angles can be resolved by RIFDS for SUAV energy calculation.
- (3) Some improvement measures are introduced to WOA to avoid local minima. The modified WOA, called IWOA, is proposed.
- (4) The traditional SUAV solar energy production is modified and recalculated according to ASHRAE Clear Sky Model and the solar irradiance calculation principle for slant surfaces.

## 2. Problem formulation

### 2.1. Obstacle modeling

The building obstacles in urban environment can mainly be described as cuboids, cylinders and their combinations. The unified formulation of obstacles is shown as follows:

$$\Gamma(\xi) = \left(\frac{x-x_0}{a}\right)^{2d} + \left(\frac{y-y_0}{b}\right)^{2e} + \left(\frac{z-z_0}{c}\right)^{2f} \quad (1)$$

where  $\xi = (x, y, z)$  is the SUAV position;  $\xi_0 = (x_0, y_0, z_0)$  is the obstacle center;  $a, b, c$  are axes lengths of the obstacle; and  $d, e, f$  are the shape parameters. If  $d = e = 1, f > 1$ , the obstacle is approximately a cylinder; if  $d > 1, e > 1, f > 1$ , the obstacle is approximately a cuboid. If  $\Gamma(\xi) > 1$ , SUAV is away from the obstacle, i.e., SUAV is safe; if  $\Gamma(\xi) < 1$ , SUAV is inside of the obstacle, i.e., SUAV is located in the no-fly zone; if  $\Gamma(\xi) = 1$ , SUAV is on the surface of the obstacle, i.e., SUAV collides with the obstacle. For path planning, the situation of  $\Gamma(\xi) \leq 1$  must be avoided. To describe the following proposed judgement method for the shadow region, according to Eq. (1), the side surface equation of the obstacle can be obtained.

### 2.2. SUAV dynamic model and constraints

According to the mission requirements, suppose that SUAV maintains a level flight at the constant height  $h_0$  and constant

speed  $V$ . The discretized 3-DOF dynamic model of SUAV is described as follows:

$$\begin{cases} \psi(t+1) = \psi(t) + g \tan(\phi(t)) \cdot \Delta T \\ x(t+1) = x(t) + V \cos(\psi(t+1)) \cdot \Delta T \\ y(t+1) = y(t) + V \sin(\psi(t+1)) \cdot \Delta T \end{cases} \quad (2)$$

where  $\psi$  and  $\phi$  are heading and bank angles respectively;  $\Delta T$  is the sampling time; and  $t$  is the current time.  $\phi$  is usually set as the control input for SUAV [1,6,7,27]. The dynamic constraint in SUAV is  $|\phi| \leq \phi_{\max}$ .

### 2.3. SUAV energy model in urban environment

#### 2.3.1. The modified received solar irradiance for SUAV

**Assumption 1.** In this paper, SUAV always flies in clear sky conditions without clouds which meets the requirements of ASHRAE Clear Sky Model.

In this paper, ASHRAE Clear Sky Model, which is widely applied in solar engineering, is introduced to modify some unreasonable aspects of the current studies on SUAV energy production processes [1,2,6-9] as follows.

The electric energy of SUAV is converted by solar cells from solar radiation. The solar irradiance  $I$  ( $\text{W}/\text{m}^2$ ), which is perpendicular to the horizontal plane in the exoatmosphere, is calculated as:

$$I = I_0 \left( 1 + 0.034 \cos \frac{2\pi n_{\text{day}}}{365.25} \right) \quad (3)$$

where  $I_0$  is the solar constant and  $n_{\text{day}}$  is the number of solar days which start from January 1 as 1.

The solar radiation can be absorbed, diffused and reflected by the atmosphere of earth. Thus, the total solar irradiance on the earth horizontal surface  $I_h$  is calculated based on the years of observation and summary as follows:

$$\begin{cases} I_h = I_b \sin \alpha_e + I_d \\ I_b = I_e^{-\tau_b m_r^b} \\ I_d = I_e^{-\tau_d m_r^d} \\ b = 1.219 - 0.043 \tau_b - 0.151 \tau_d - 0.204 \tau_b \tau_d \\ d = 0.202 + 0.852 \tau_b - 0.007 \tau_d - 0.357 \tau_b \tau_d \\ m_r = \frac{1}{\sin \alpha_e} \end{cases} \quad (4)$$

where  $I_b$  and  $I_d$  are the beam and diffuse irradiances on the earth horizontal surface;  $\tau_b$  and  $\tau_d$  are the beam and the diffuse optical depths respectively, whose values can be obtained by [11];  $b$  and  $d$  are the beam and the diffuse air mass exponents respectively;  $m_r$  is the air mass ratio; and  $\alpha_e$  is the solar elevation angle.

As time goes on, the solar elevation angle  $\alpha_e$  and solar azimuth angle  $\alpha_z$  can be calculated as follows:

$$\begin{cases} \sin \alpha_e = \sin n_{\text{lat}} \sin \delta + \cos n_{\text{lat}} \cos \delta \cos \omega(t) \\ \sin \alpha_z = \frac{\cos \delta \cos \omega(t)}{\cos \alpha_e} \\ \delta = 0.4093 \sin \left( \frac{2\pi(284+n_{\text{day}})}{365} \right) \\ \omega(t) = 0.2618 \times (12 - t_{\text{local}}) \end{cases} \quad (5)$$

where  $n_{\text{lat}}$  is the latitude;  $\delta$  is the declination angle of the sun;  $t_{\text{local}}$  is the current hour of the day; and  $\omega(t)$  is the hour of sun.

Then, to obtain the solar irradiance on the wings of SUAV, the incident angle  $\lambda$  of the sunlight on the surface of the wings should be calculated. As shown in Fig. 1, P-NED is the navigation coordinate frame fixed to the ground, which points to the orientations of north, east and the ground, respectively. The unit vector of the sunlight  $\mathbf{V}_p$  in the navigation coordinate frame is expressed as

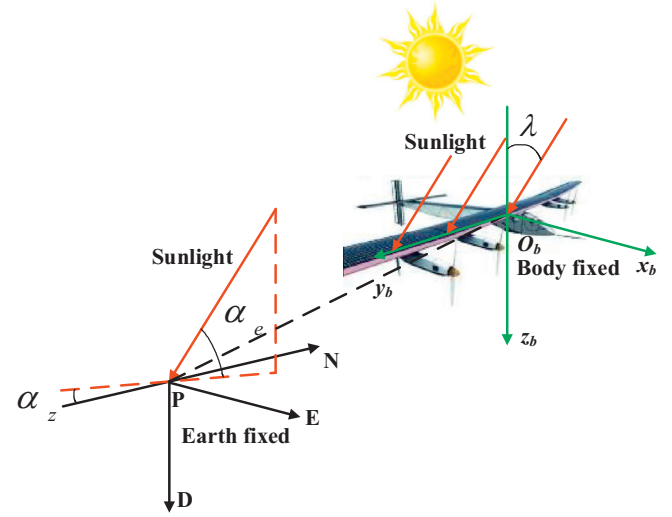


Fig. 1. The geometrical relationship between the sun and SUAV.

$$\mathbf{V}_p = \begin{bmatrix} \cos \alpha_e \cos \alpha_z \\ \cos \alpha_e \sin \alpha_z \\ -\sin \alpha_e \end{bmatrix} \quad (6)$$

The unit vector  $\mathbf{V}_b$  along the reverse direction of Axis  $O_b z_b$  in the body fixed frame is expressed as

$$\mathbf{V}_b = [0 \quad 0 \quad -1]^T \quad (7)$$

$\mathbf{V}_p$  can be converted under the body fixed coordinate frame in the following form:

$$\mathbf{V}_p^b = \mathbf{L}_x(\phi) \mathbf{L}_y(\theta) \mathbf{L}_z(\psi) \begin{bmatrix} \cos \alpha_e \cos \alpha_z \\ \cos \alpha_e \sin \alpha_z \\ -\sin \alpha_e \end{bmatrix} \quad (8)$$

where  $\theta$  is the flight path angle and  $\mathbf{L}_x$ ,  $\mathbf{L}_y$ ,  $\mathbf{L}_z$  are the element rotation matrixes. Because SUAV maintains a level flight,  $\theta$  can be regarded as zero.

According to vector multiplication,  $\cos \lambda$  is calculated as

$$\begin{aligned} \cos \lambda = \mathbf{V}_b \cdot \mathbf{V}_p^b &= \cos \alpha_e \sin \alpha_z \cos \psi \sin \phi \\ &\quad - \cos \alpha_e \cos \alpha_z \sin \psi \sin \phi + \sin \alpha_e \cos \phi \end{aligned} \quad (9)$$

Finally, the solar irradiance on the surface of the wings  $P_{UAV}$  can be worked out. In the traditional studies on SUAV energy production process [1,2,6-9],  $P_{UAV}$  is calculated as

$$P_{UAV} = \begin{cases} P_{sd} \cos \lambda & \text{if } \cos \lambda \geq 0 \\ 0 & \text{if } \cos \lambda < 0 \end{cases} \quad (10)$$

where  $P_{sd}$  is the solar spectral density and is regarded as a constant. However, according to our analysis of the solar irradiance in Eq. (4), there are three kinds of solar radiation absorbed by the wings:  $I_h$ ,  $I_b$  and  $I_d$ . Therefore,  $P_{UAV}$  in Eq. (10) cannot represent the influence of the different types of solar radiations comprehensively. Thus, another way should be found to rewrite the equation of  $P_{UAV}$ .

**Remark 1.** When  $\cos \lambda < 0$ , the lower surface of the wings is irradiated by solar radiation. However, the cells of the SUAV mentioned in [1] are only installed on the upper wing surface. Hence, the produced power is zero.

The surface of the wings can be regarded as a piece of flying slant solar panel. The absorbed radiation can be calculated according to the solar irradiance calculation principle for slant surfaces as follow, which is widely utilized in the solar engineering

industry [10]:

$$\begin{cases} P_{UAV} = P_b + P_d + P_r \\ P_b = \begin{cases} I_b \cos \lambda & \text{if } \cos \lambda \geq 0 \\ 0 & \text{if } \cos \lambda < 0 \end{cases} \\ P_d = I_d \cos^2 \frac{\phi}{2} \\ P_r = \rho_r I_r \sin^2 \frac{\phi}{2} \end{cases} \quad (11)$$

where  $P_b$ ,  $P_d$ , and  $P_r$  are the beam irradiance, the diffuse irradiance, and the ground reflection irradiance on the airfoil respectively; and  $\rho_r$  is the ground reflection factor. Compared with the previous energy modeling method in Eq. (10), the modified Eq. (11) is more accurate.

### 2.3.2. Energy collection and consumption models of SUAV

When sunlight shines on solar cells on wings, cells produce the electric power  $P_{in}$ :

$$P_{in} = \eta_{sol} S P_{UAV} \quad (12)$$

where  $\eta_{sol}$  is the efficiency of the solar cells and  $S$  is the area of the wings.

Hence, the collected energy is

$$E_{in} = \int_{t_0}^{t_f} P_{in} dt \quad (13)$$

Then, the energy consumption power  $P_{out}$  is calculated as the same as [1]:

$$\begin{cases} P_{out} = \frac{TV}{\eta_{prop}} + P_E \\ T = D \\ D = \frac{1}{2} \rho V^2 S C_D \\ C_D = C_{D0} + \frac{C_L^2}{\varepsilon \pi R_a} \\ C_L = \frac{2mg}{\rho V^2 S \cos \phi} \end{cases} \quad (14)$$

where  $T$  is the thrust;  $\eta_{prop}$  is the efficiency of the propeller;  $P_E$  is the consumed power of the airborne equipment, which can be considered as a constant;  $D$  is the drag;  $\rho$  is the air density;  $C_D$  is the coefficient of drag;  $C_{D0}$  is the parasitic drag coefficient;  $C_L$  is the coefficient of lift;  $\varepsilon$  is the Oswald efficiency factor; and  $R_a$  is the ratio of the wings.

Hence, the consumed energy is

$$E_{out} = \int_{t_0}^{t_f} P_{out} dt \quad (15)$$

Therefore, the total energy is

$$E_{total} = E_{in} - E_{out} \quad (16)$$

### 2.3.3. Judgment method for the shadow region

When SUAV flies among high buildings, the buildings higher than SUAV may block out sunlight for SUAV. If the sunlight is blocked out, i.e., SUAV is located in the shadow region, the collected power  $P_{in}$  can be regarded as zero.

In the fields of urban planning and construction design, the shadow regions for the rated altitude can be obtained via the methodologies of computer graphics and numerical simulations [28,29]. The advantages of these methodologies are their precision and ability to calculate all kinds of irregular buildings. However, their disadvantages are very obvious: the precise simulation will require a large amount of computing resources, which will make the optimization problem too complicated. Hence, a simple and practical judgment method for identifying the shadow region is proposed as follows:

**Step. 1.** Obtain the equation of sunlight. Suppose that the position of SUAV is  $(x_u, y_u, h_u)$ . According to Eq. (6), the straight-line equation of the sunlight which points to SUAV can be written in two-point form:

$$\frac{x_u - x}{\cos \alpha_e \cos \alpha_z} = \frac{y_u - y}{\cos \alpha_e \sin \alpha_z} = \frac{h_u - h}{-\sin \alpha_e} \quad (17)$$

**Step. 2.** Judge whether there is an intersection between the straight-line equation of the sunlight and the side surface equations of the buildings higher than SUAV. We combine Eq. (17) with the side surface equation of each obstacle according to Eq. (1), and judge whether there is an intersection. The schematic diagram is shown in Fig. 2.

**Step. 3.** Decide the input power of SUAV. If there is no intersection on the side surface,  $P_{in}$  is calculated by Eq. (12). Instead, let  $P_{in} = 0$ .

## 3. Restrained Interfered Fluid Dynamical System

### 3.1. IFDS

Suppose that the destination is  $\xi_d = (x_d, y_d, z_d)$  and the number of the obstacles is  $K$ .

First, the original fluid speed  $\mathbf{u}$  is described as

$$\mathbf{u} = - \left[ \frac{V(x - x_d)}{d} \quad \frac{V(y - y_d)}{d} \quad \frac{V(z - z_d)}{d} \right]^T \quad (18)$$

where  $d = \sqrt{(x - x_d)^2 + (y - y_d)^2 + (z - z_d)^2}$  is the distance between SUAV and its destination.

Then, the influence of the obstacles on the original fluid speed is expressed by the total interfered modulation matrix  $\tilde{\mathbf{M}}$ :

$$\tilde{\mathbf{M}} = \sum_{k=1}^K \omega_k \mathbf{M}_k \quad (19)$$

where  $\omega_k$  is the weighting coefficient of the  $k$ th obstacle and  $\mathbf{M}_k$  is the interfered modulation matrix of the  $k$ th obstacle.  $\omega_k$  and  $\mathbf{M}_k$  are defined as

$$\omega_k = \begin{cases} 1 & K = 1 \\ \prod_{i=1, i \neq k}^K \frac{(\Gamma_i - 1)}{(\Gamma_i - 1) + (\Gamma_k - 1)} & K \neq 1 \end{cases} \quad (20)$$

$$\mathbf{M}_k = \mathbf{I} - \frac{\mathbf{n}_k \mathbf{n}_k^T}{|\Gamma_k|^{1/\rho_k} \mathbf{n}_k^T \mathbf{n}_k} + \frac{\mathbf{t}_k \mathbf{n}_k^T}{|\Gamma_k|^{1/\sigma_k} \|\mathbf{t}_k\| \|\mathbf{n}_k\|} \quad (21)$$

where  $\Gamma_k$  and  $\Gamma_i$  are the obstacle equations calculated by Eq. (1);  $\mathbf{I}$  is the three-order unit matrix;  $-\frac{\mathbf{n}_k \mathbf{n}_k^T}{|\Gamma_k|^{1/\rho_k} \mathbf{n}_k^T \mathbf{n}_k}$  and  $\frac{\mathbf{t}_k \mathbf{n}_k^T}{|\Gamma_k|^{1/\sigma_k} \|\mathbf{t}_k\| \|\mathbf{n}_k\|}$  are the repulsive and tangential matrixes, respectively;  $\rho_k$  and  $\sigma_k$  are the repulsive and tangential parameters, respectively;  $\mathbf{n}_k = \left[ \frac{\partial \Gamma_k}{\partial x} \quad \frac{\partial \Gamma_k}{\partial y} \quad \frac{\partial \Gamma_k}{\partial z} \right]^T$  is the normal vector; and  $\mathbf{t}_k$  is the tangent vector, which can be obtained as follows.

The tangent reference frame  $o'-x'y'z'$  is established by taking  $\mathbf{t}_{k,1}$ ,  $\mathbf{t}_{k,2}$  and  $\mathbf{n}_k$  as the  $x'$  axis,  $y'$  axis and  $z'$  axis respectively.

$$\begin{cases} \mathbf{t}_{k,1} = \left[ \frac{\partial \Gamma_k}{\partial y} & -\frac{\partial \Gamma_k}{\partial x} & 0 \right]^T \\ \mathbf{t}_{k,2} = \left[ \frac{\partial \Gamma_k}{\partial x} \frac{\partial \Gamma_k}{\partial z} & \frac{\partial \Gamma_k}{\partial y} \frac{\partial \Gamma_k}{\partial z} & -\left( \frac{\partial \Gamma_k}{\partial x} \right)^2 - \left( \frac{\partial \Gamma_k}{\partial y} \right)^2 \right]^T \end{cases} \quad (22)$$

Hence, any tangent vector from the tangent plane can be expressed as

$$\mathbf{t}'_k = [\cos \theta_k \quad \sin \theta_k \quad 0]^T \quad (23)$$

where  $\theta_k \in [-\pi, \pi]$  is the tangential direction coefficient, which is the rotary angle along the  $z'$  axis. Then, in the inertial frame,  $\mathbf{t}'_k$  can be transformed to  $\mathbf{t}_k$ :

$$\mathbf{t}_k = \mathbf{\Omega}_T^I \mathbf{t}'_k \quad (24)$$

where  $\mathbf{\Omega}_T^I$  is the coordinate transformation matrix from the tangent reference frame to the inertial frame.

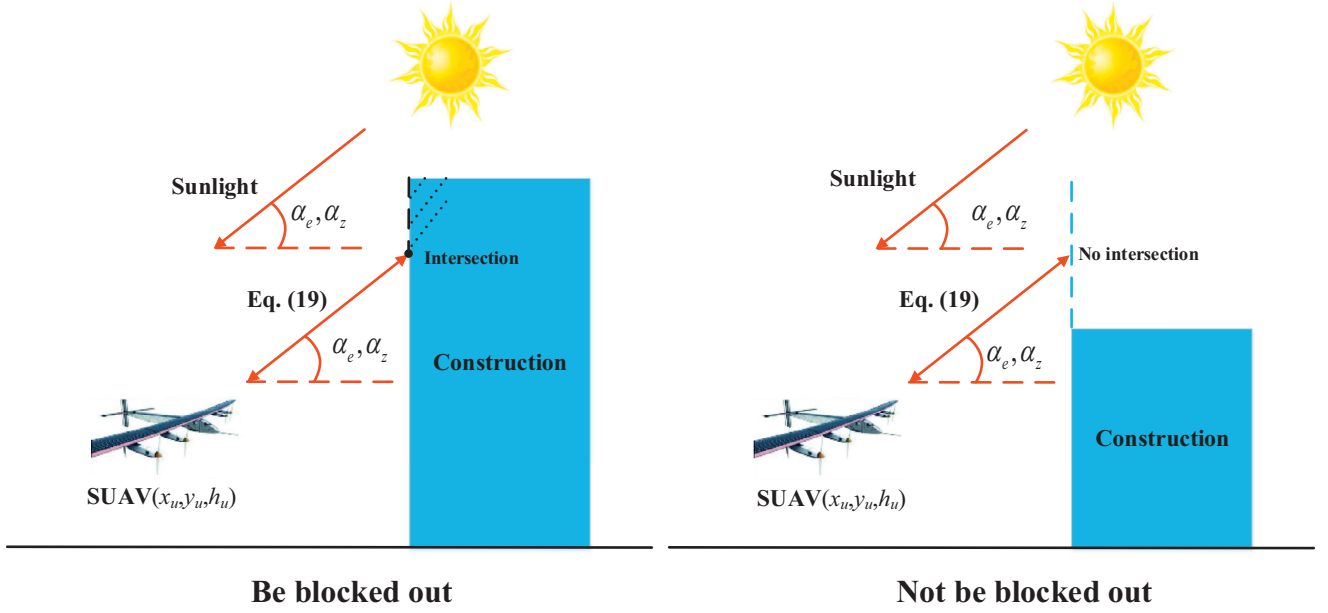


Fig. 2. The schematic diagram of the judgment method.

Moreover, for the building obstacles, the disturbed fluid speed  $\tilde{\mathbf{u}}$  can be obtained by modifying the original fluid speed  $\mathbf{u}$ :

$$\tilde{\mathbf{u}} = \tilde{\mathbf{M}}\mathbf{u} \quad (25)$$

Finally, the next planned waypoint is obtained by

$$\mathbf{P}_{t+1} = \mathbf{P}_t + \tilde{\mathbf{u}} \cdot \Delta T \quad (26)$$

The purpose of introducing the tangential matrix is to avoid the stagnation point and trap area problems. The parameters  $\rho_k$ ,  $\sigma_k$  and  $\theta_k$  determine the shape of the streamline. By adjusting  $\sigma_k$  and  $\theta_k$ , the streamline can get rid of the stagnation point and trap area problems. The extent of the reaction to obstacles can be adjusted by  $\rho_k$  and  $\sigma_k$ . The bigger  $\rho_k$  or  $\sigma_k$  is, the earlier and more drastically the path avoids the obstacles.

**Remark 2.** Because the buildings are the static obstacles, the disturbed fluid speed can be calculated as Eq. (25). If the obstacles are dynamic with speed vector  $\mathbf{v}$ ,  $\tilde{\mathbf{u}}$  should be recalculated as  $\tilde{\mathbf{u}} = \tilde{\mathbf{M}}(\mathbf{u} - \mathbf{v}) + \mathbf{v}$ .

### 3.2. RIFDS

According to Eq. (26), the planned path of the traditional IFDS is totally divorced from UAV model. Hence, Restrained IFDS (RIFDS) is proposed in this paper to guarantee the feasibility of the planned path.

Suppose the current heading angle is  $\psi(t)$ . The disturbed fluid speed is the expected speed, i.e., the command speed in the next moment, which can be written as  $\tilde{\mathbf{u}}(t) = [\tilde{u}_x(t) \ \tilde{u}_y(t) \ \tilde{u}_z(t)]^T$  ( $\tilde{u}_z(t) = 0$ ). Hence, the expected heading angle is calculated as

$$\psi_c(t) = \tan^{-1} \left( \frac{\tilde{u}_z(t)}{\|\tilde{\mathbf{u}}(t)\|} \right) \quad (27)$$

The expected heading angular rate is

$$\dot{\psi}_c(t) = \frac{\psi_c(t) - \psi(t)}{\Delta T} \quad (28)$$

**Remark 3.** The range of the difference value  $(\psi_c(t) - \psi(t))$  should be within  $(-\pi, \pi]$ . Hence, in the actual programming, the

difference value should be discussed according to the different quadrants.

Put  $\dot{\psi}_c(t)$  into Eq. (1), and the expected bank angle  $\phi_c(t)$  can be resolved:

$$\phi_c(t) = \tan^{-1} \left( \frac{\dot{\psi}_c(t)}{g} \right) \quad (29)$$

The resolved  $\phi_c(t)$  should satisfy the constraint condition as  $|\phi(t)| \leq \phi_{\max}$ . Hence, the actual restrained bank angle  $\phi_a(t)$  is calculated as

$$\phi_a(t) = \begin{cases} \phi_c(t) & \text{if } \phi_c(t) \leq |\phi_{\max}| \\ \phi_{\max} & \text{if } \phi_c(t) > \phi_{\max} \\ -\phi_{\max} & \text{if } \phi_c(t) < -\phi_{\max} \end{cases} \quad (30)$$

Then, put  $\phi_a(t)$  back into Eq. (1) as the control input. The position of the next planned waypoint and the actual feasible heading angle can be resolved.

By introducing the constraint of the bank angle and the UAV dynamic model as Eq. (1), RIFDS can overcome the defect of the traditional IFDS being divorced from the SUAV model. In addition, the elements for calculating the received solar energy,  $\psi$  and  $\phi$ , can be resolved (see Eq. (9)). The rationality of RIFDS can be shown in the following case: Suppose that UAV turns in the level plane by IFDS and RIFDS, respectively. The initial position and the destination of the UAV are  $(0, 0, 150)$  and  $(-300, 0, 150)$ , respectively. The initial speed direction of the UAV points in the positive direction of the X-axis (i.e.,  $\gamma = 0$  and  $\chi = 0$ ). The rolling angle is limited to  $|\phi| \leq 45^\circ$ . The comparison of the flight trajectories by the two methods is shown in Fig. 3.

In Fig. 3, the trajectory by IFDS points in the rear destination directly, which is divorced from the actual dynamic model of UAV. In contrast, the trajectory by RIFDS has a gradual turning process to the rear destination that considers the dynamic model and constraints. Hence, RIFDS is more rational than IFDS.

## 4. Improved Whale Optimization Algorithm

### 4.1. Whale Optimization Algorithm

WOA is a novel heuristic algorithm that mimics the hunting behavior of the humpback whale. In WOA, the position of each whale

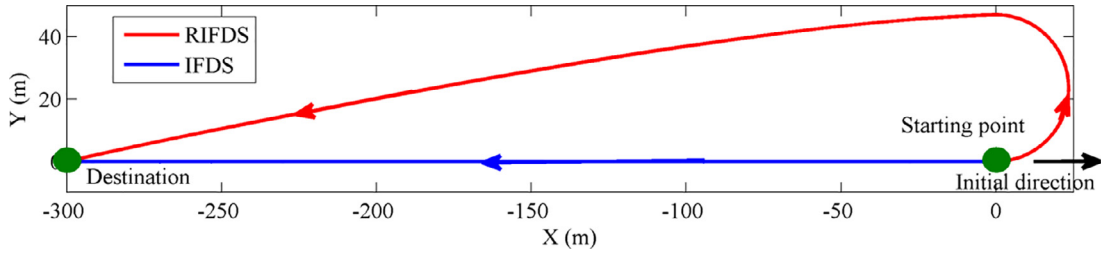


Fig. 3. The flight trajectories of a UAV turns in a level plane by IFDS and RIFDS.

represents a feasible solution. The framework of WOA is divided into three parts as follows.

#### (1) Encircling prey

WOA assumes that the current best candidate solution is the target prey or is close to the optimum. After the best search agent is defined, the other search agents will try to update their positions toward the best search agent. This behavior is represented as follows:

$$\begin{cases} \mathbf{D} = |\mathbf{C}\mathbf{X}^*(t) - \mathbf{X}(t)| \\ \mathbf{X}(t+1) = \mathbf{X}^*(t) - \mathbf{A}\mathbf{D} \end{cases} \quad (31)$$

where  $t$  is the current iteration;  $\mathbf{X}^*(t)$  is the position vector of the current best search agent, i.e., the agent with the best fitness;  $\mathbf{X}(t)$  is the position vector of the current agent;  $A$  and  $C$  are the parameters calculated as

$$\begin{cases} A = 2ar_1 - a \\ C = 2r_2 \\ a = 2 - 2t/T_{\max} \end{cases} \quad (32)$$

where  $r_1$  and  $r_2$  are random numbers in  $(0, 1)$ ;  $a$  is linearly decreased from 2 to 0; and  $T_{\max}$  is the maximum iteration.

#### (2) Bubble-net attacking method

Whales move toward the target via a spiral motion whose mathematical formula is

$$\begin{cases} \mathbf{X}(t+1) = \mathbf{X}^*(t) + \mathbf{D}_p e^{bl} \cos(2\pi l) \\ \mathbf{D}_p = |\mathbf{X}^*(t) - \mathbf{X}(t)| \end{cases} \quad (33)$$

where  $\mathbf{D}_p$  is the distance vector between the whales and the target;  $b$  is a constant for defining the shape of the logarithmic spiral; and  $l$  is a random number in  $[-1, 1]$ .

Because whales swim around their prey within a shrinking circle and along a spiral-shaped path simultaneously, a probability of 50% is assumed when choosing between the shrinking encircling mechanism and the spiral model to update the position of whales during the optimization. The mathematical model is as follows:

$$\begin{cases} \mathbf{X}(t+1) = \mathbf{X}^*(t) - \mathbf{A}\mathbf{D} & \text{if } p < .5 \\ \mathbf{X}(t+1) = \mathbf{X}^*(t) + \mathbf{D}_p e^{bl} \cos(2\pi l) & \text{if } p \geq .5 \end{cases} \quad (34)$$

where  $p$  is a random number in  $[0, 1]$ .

When the whales prey and close to the target,  $a$  will decrease from 2 to 0. The fluctuation range of  $A$  will decrease following  $a$  in  $[-a, a]$ . When  $A$  is in  $[-1, 1]$ , the next position of the whale can be anywhere between itself and the target. Therefore, when  $A < 1$ , whales are set to attack the target.

#### (3) Search for prey

When whales are searching for prey, the mathematical formula is shown as follows:

$$\begin{cases} \mathbf{D} = |\mathbf{C}\mathbf{X}_{rand}(t) - \mathbf{X}(t)| \\ \mathbf{X}(t+1) = \mathbf{X}_{rand}(t) - \mathbf{A}\mathbf{D} \end{cases} \quad (35)$$

where  $\mathbf{X}_{rand}(t)$  is the randomly selected position vector of the whale. When  $A \geq 1$ , WOA will select a search agent randomly. According to the randomly selected position, the whale can be forced to deviate from the current target and find a more proper one. This will enhance the global searching ability.

The optimization process of WOA can be summarized as follows: First, produce  $N$  whale agents randomly as the initial population in the search space. Then, update the position of each agent according to the current best agent or a randomly selected agent. Moreover, determine the motion forms of the whales (including the spiral motion and the encircling motion) according to the random number  $p$ . Finally, loop the iteration until the termination condition is satisfied.

### 4.2. Improved WOA

To balance the global and the local searching, the setting of  $A$  is introduced in WOA. The local optimum problem can be avoided to some extent. However, because the searching process is completely dependent on the randomness, the searching efficiency is not highly satisfactory. The randomness still easily results in the local optimum. To overcome the noted drawback, the adaptive Chaos-Gaussian switching solving strategy and the coordinated decision-making strategy are introduced to WOA, and Improved WOA (IWOA) is proposed in this paper.

#### 4.2.1. Adaptive chaos-Gaussian switching solving strategy

To enhance the global searching ability, chaos is introduced to WOA. Chaos is a nonlinear phenomenon that exists widely in nature. It has the characteristics of randomness and ergodicity. Hence, chaos is often combined with other IOAs to improve their global searching abilities [30–32]. In this paper, we adopt Logistic chaos equation:

$$\begin{aligned} \beta_j(\tau+1) &= \mu_0 \beta_j(\tau)(1 - \beta_j(\tau)), \\ \beta_j(\tau) &\in (0, 1), \beta_j(\tau) \neq 0.25, 0.5, 0.75. \end{aligned} \quad (36)$$

where  $\beta_j$  is the chaotic iteration variable and  $\tau$  is the number of chaotic iteration. When  $\mu_0 = 4$ , Logistic equation is in a complete chaos state. Fig. 4 shows the Logistic chaos distribution character of the two-dimensional vector with 500 iterations.

From Fig. 4, the agents scatter across the whole search space and have a higher probability of being mainly concentrated on the edge area (the red circle area). Hence, the chaos is beneficial for WOA to jump out of the local optimum.

In contrast, to enhance the local searching ability, a probability density function with centrality should be introduced to WOA. Instinctively, we select Gaussian distribution  $N(\mu, \sigma^2)$ , whose probability density function is

$$f(x) = \frac{1}{\sqrt{2\pi}\sigma} \exp\left(-\frac{(x-\mu)^2}{2\sigma^2}\right), \sigma > 0. \quad (37)$$

where  $\mu$  is the Gaussian expectation and  $\sigma^2$  is the variance.

To intuitively show that Gaussian distribution character is beneficial for the local searching, we select another typical distribution:

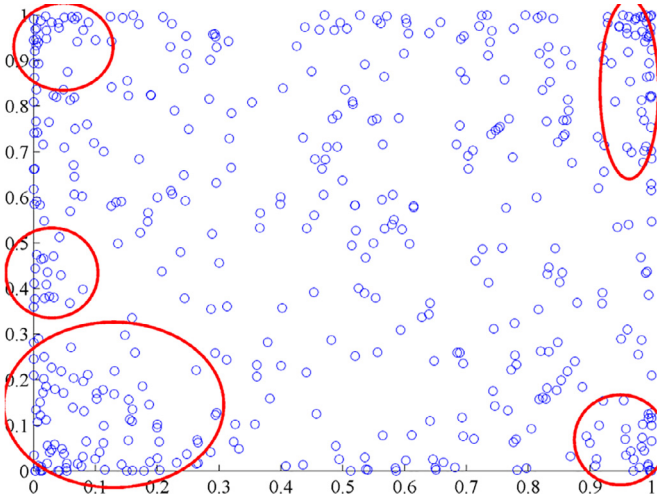


Fig. 4. Logistic chaos distribution character.

exponential distribution [33,34] as the comparative item. Fig. 5 shows the normalized Gaussian distribution character  $N^*(0, 1)$  (i.e., standard normal distribution) and exponential distribution character of the two-dimensional position vector.

From Fig. 5, the agents in Gaussian distribution are concentrated on the central area (the red circle area) with a higher probability, which is beneficial for the local searching ability. Hence, the searching precision will be improved accordingly. On the contrary, the agents in exponential distribution only concentrate on the bottom-left corner (the green circle area) in the search space. It can neither enhance the local searching ability like Gaussian distribution nor have the ergodicity to enhance the global searching ability like chaos.

Therefore, after the performance analysis, the corresponding strategy is designed for WOA as follows:

**Step. 1.** Population initialization.

**Step. 2.** Execute WOA in the first step and generate the fitness value of each position.

**Step. 3.** According to the conditions of the population, determine whether to select the chaos variation operation from Eq. (38) with  $\varepsilon$  iterations or the Gaussian variation operation from Eq. (39) to update the initialization positions of the agents to be used for executing WOA in the next iteration.

$$\begin{cases} \mathbf{X}_j(t) = (1 - \zeta)\mathbf{X}_j(t) + \zeta\delta_C \\ \delta_C = \mathbf{X}^{\min} + \beta_j(\varepsilon + 1)(\mathbf{X}^{\max} - \mathbf{X}^{\min}) \end{cases} \quad (38)$$

$$\begin{cases} \mathbf{X}_j(t) = (1 - \zeta)\mathbf{X}_j(t) + \zeta\delta_G \\ \delta_G = \mathbf{X}^{\min} + N^*(0, 1)(\mathbf{X}^{\max} - \mathbf{X}^{\min}) \end{cases} \quad (39)$$

where  $\mathbf{X}^{\max}$  and  $\mathbf{X}^{\min}$  are the upper and lower bound vectors of  $\mathbf{X}_j(t)$ ;  $\delta_C$  and  $\delta_G$  are the chaos and Gaussian variation operators;  $\beta_j(\varepsilon + 1)$  is the chaotic iteration value obtained by Eq. (36) with  $\varepsilon$  iterations from a random number  $\beta_j(1) \in (0, 1)$ ; and  $\zeta$  is the shrinking factor to determine the variation space, which is calculated as

$$\zeta = 1 - \left| \frac{t-1}{t} \right|^m \quad (40)$$

where  $m$  is utilized to control the shrinking speed.

**Step. 4.**  $t = t + 1$ , and return to **Step. 2.** until the maximum iteration.

In **Step. 3.**, the selection of the variation method is dependent on the condition of the population. In this paper, it can be regarded

as the improvement rate ( $IR$ ) of the population which is calculated as  $IR = N_b/N$ , where  $N_b$  is the number of the agents which are better than their last generation.  $IR$  can be utilized to measure the healthy development level of the population. Biological studies show that when  $IR$  remains at 20% approximately, this condition is the most favorable to population growth [35]. If  $IR$  is too low, the search space is large enough to avoid the local optimum but the searching precision is low; namely, the local searching ability is weak. Thus, for this condition, the Gaussian variation operation should be selected because of its centered distribution character. If  $IR$  is too high, the search space is overly concentrated in the local area; namely, the global searching ability is weak. Thus, for this condition, the chaos variation operation should be selected due to its ergodicity. Therefore, the variation method selection mechanism is designed as

$$\begin{cases} \mathbf{X}_j(t) = (1 - \zeta)\mathbf{X}_j(t) + \zeta\delta_G & IR < 0.15 \\ \mathbf{X}_j(t) = \mathbf{X}_j(t) & IR \in [0.15, 0.25] \\ \mathbf{X}_j(t) = (1 - \zeta)\mathbf{X}_j(t) + \zeta\delta_C & IR > 0.25 \end{cases} \quad (41)$$

where the setting of the interval  $[0.15, 0.25]$  is done to avoid an overly frequent switch of variation methods.

#### 4.2.2. Coordinated decision-making mechanism

In GWO proposed by [24], the population is divided into four hierarchies:  $\alpha$ ,  $\beta$ ,  $\delta$  and  $\omega$ .  $\alpha$ ,  $\beta$  and  $\delta$  are the ones that have the top three optimal fitness values. The search direction of the population is codetermined by  $\alpha$ ,  $\beta$  and  $\delta$ . The practical experiments indicate that such elite agents coordinated decision-making mechanism can make the population jump out of the local optimum to some extent. Hence, such mechanism is introduced to Eq. (34) in WOA as follows:

$$\begin{cases} \mathbf{X}(t+1) = \frac{\mathbf{X}^{1*}(t) + \mathbf{X}^{2*}(t) + \mathbf{X}^{3*}(t)}{3} - \mathbf{AD} & \text{if } p < .5 \\ \mathbf{X}(t+1) = \frac{\mathbf{X}^{1*}(t) + \mathbf{X}^{2*}(t) + \mathbf{X}^{3*}(t)}{3} + \mathbf{D}_p e^{bl} \cos(2\pi l) & \text{if } p \geq .5 \\ \mathbf{D} = \left| \frac{\mathbf{X}^{1*}(t) + \mathbf{X}^{2*}(t) + \mathbf{X}^{3*}(t)}{3} - \mathbf{X}(t) \right| \\ \mathbf{D}_p = \left| \frac{\mathbf{X}^{1*}(t) + \mathbf{X}^{2*}(t) + \mathbf{X}^{3*}(t)}{3} - \mathbf{X}(t) \right| \end{cases} \quad (42)$$

where  $\mathbf{X}^{1*}(t)$ ,  $\mathbf{X}^{2*}(t)$  and  $\mathbf{X}^{3*}(t)$  are the agents with the top three optimal fitness values in each iteration.

## 5. Description of path planning

### 5.1. Path planning framework

The path planning process can be described as follows:

First, calculate the cost function  $J$  to evaluate the quality of the generated path.  $J$  is composed of several subfunctions that represent the safety, energy reserve, path length, etc. as follows:

$$J = \sum_{i=1}^G \lambda_i J_i^{sub} \quad (43)$$

where  $G$  is the number of subfunctions;  $\lambda_i$  and  $J_i^{sub}$  are the corresponding weight and subfunction, respectively.

Then, the reactive parameters of all  $K$  obstacles are optimized to obtain the minimum  $J$  by the proposed IWOA:

$$\{\rho'_1, \sigma'_1, \theta'_1, \dots, \rho'_K, \sigma'_K, \theta'_K\} = \arg \min_{\rho, \sigma, \theta} J \quad (44)$$

where  $\{\rho'_1, \sigma'_1, \theta'_1, \dots, \rho'_K, \sigma'_K, \theta'_K\}$  are the optimized reactive parameters of all  $K$  obstacles. These reactive parameters determine the trend of the planned path.

Finally, select the path with the minimum  $J$  as the flight path. For the application of SUAV in urban environment, RIFDS, IWOA, and accurate energy modeling bond together. The integrated flow diagram of the proposed path planning framework is shown in Fig. 6.

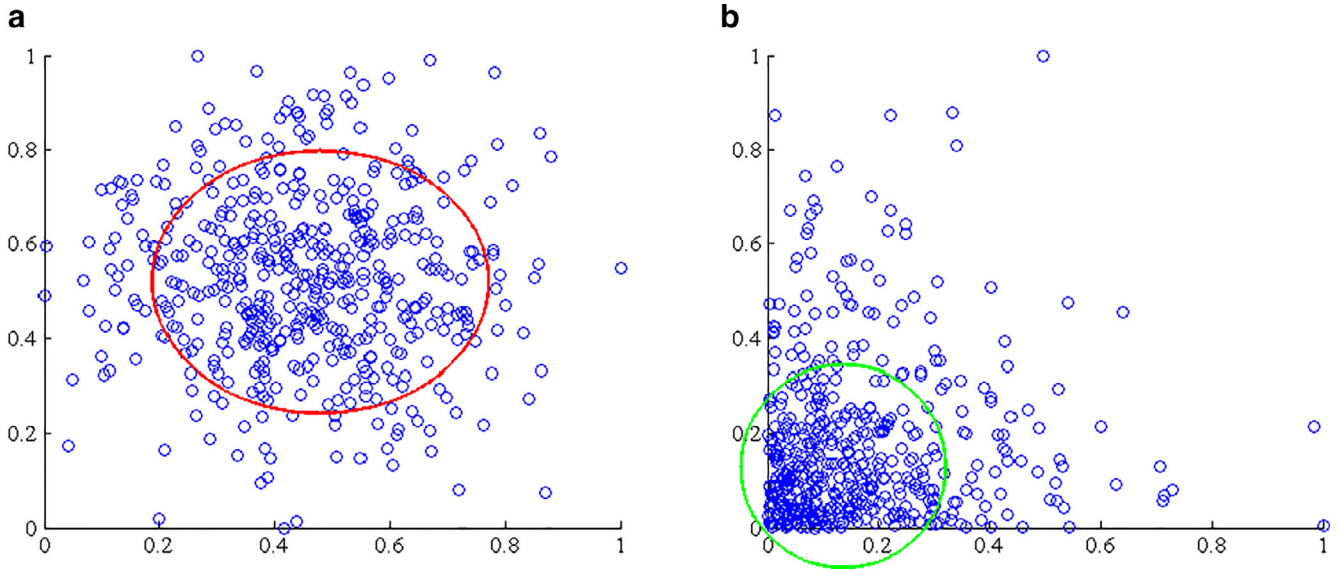


Fig. 5. The comparison between the normalized Gaussian distribution character and exponential distribution character of the two-dimensional position vector: (a) Gaussian distribution character. (b) Exponential distribution character.

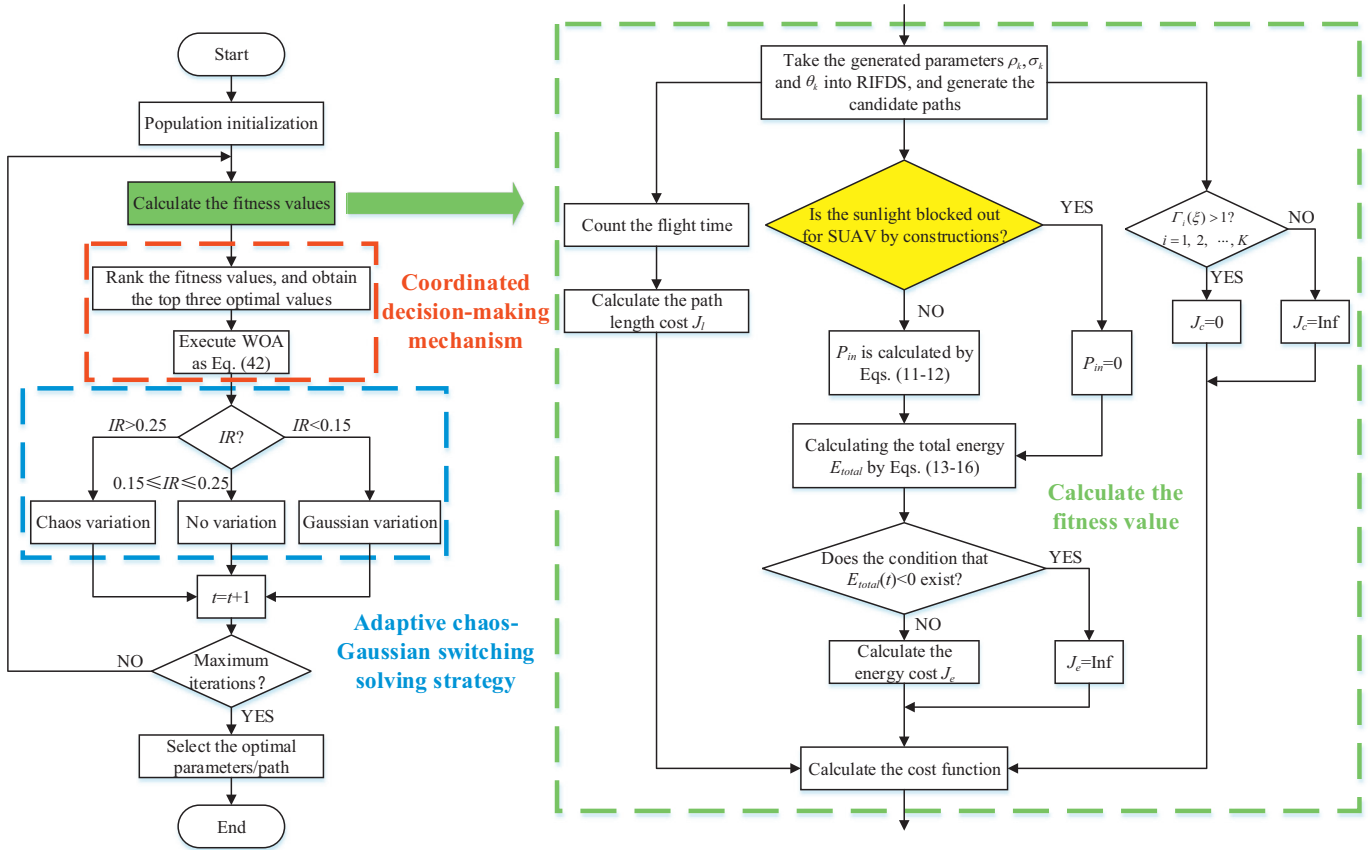


Fig. 6. The integrated flow diagram of the proposed path planning framework.

5.2. Cost function

The cost function is composed of the collision index  $J_c$ , the energy index  $J_e$  and the path length index  $J_l$ .

The collision index describes the performance of SUAV in avoiding high buildings in urban environment, which is defined as

$$J_c = \begin{cases} 0 & \forall \Gamma_i(\xi) > 1, i = 1, 2, \dots, K \\ +\infty & \exists \Gamma_i(\xi) \leq 1, i = 1, 2, \dots, K \end{cases} \quad (45)$$

where  $\Gamma_i(\xi)$  is defined in Eq. (1).

The energy index describes the energy storage condition of SUAV, which is defined as

$$J_e = \begin{cases} -E_{total} & \forall E_{total}(t) \geq 0 \\ +\infty & \exists E_{total}(t) < 0 \end{cases} \quad (46)$$

where  $E_{total}$  represents the total energy of the whole flight process and  $E_{total}(t)$  represents the total energy in the moment  $t$ . The meaning of  $J_e$  is that SUAV should store as much energy as possible

**Table 1**  
The simulation parameters.

| Parameter   | Value                              |
|---|------------------------------------|
| Sampling time, $\Delta T$ (s)                         | 0.1                                |
| Flight speed (m/s)                                    | 20                                 |
| Flight height (m)                                     | 150                                |
| Starting point  | (0, 0, 150)                        |
| Destination   | (750, 750, 150)                    |
| Maximum rolling angle, $\phi_{max}$ (deg)             | 60                                 |
| SUAV parameters                                       | From [1]                           |
| Location in simulation scenario                       | Beijing, China (39.93°N, 116.28°E) |
| Date in simulation scenario                           | 12:00 a.m., Mar. 1st               |
| Ground reflection factor, $\rho_r$                    | 0.2                                |
| SUAV initial energy storage (J)                       | 20                                 |
| Range of repulsive reaction coefficient, $\rho_k$     | [0.1, 20]                          |
| Range of tangential reaction coefficient, $\sigma_k$  | [0.1, 20]                          |
| Range of tangential direction coefficient, $\theta_k$ | [0, $\pi$ ]                        |
| Population size, $N$                                  | 100                                |
| Maximum iteration, $T_{max}$                          | 100                                |
| Shrink speed control factor, $m$                      | 1                                  |

**Table 2**  
The simulation results.

|                          | Total flight time (s) | Total energy (J) |
|--------------------------|-----------------------|------------------|
| The proposed framework   | 54.4                  | 143.16           |
| Time optimal framework   | 53.6                  | 26.93            |
| Energy optimal framework | 56.9                  | 330.04           |

under the condition that the produced energy is always positive to maintain the normal control.

The path length index reflects the mission accomplishment quality directly, i.e., the core mission of SUAV is to arrive at its destination as soon as possible. Because the flight speed is set as a constant, the total time  $t_{total}$  when SUAV arrives at its destination can be utilized to measure the flight path length. The smaller  $t_{total}$  is, the better the mission accomplishment quality is. The path length index is defined as

$$J_l = t_{total} \tag{47}$$

**Remark 4.** In Eq. (46), the reason why  $J_e = +\infty$  when the total energy of SUAV is less than zero is in consideration of the worst situation i.e., the rechargeable batteries in SUAV do not contain any stored electric energy at all.

**Remark 5.** In this paper, we suppose that when the condition  $d < 5m$  appears, SUAV can be considered to arrive at its destination.

## 6. Simulation

### 6.1. Testing the performance of the proposed framework

The comparative items are set as follows: (1) The proposed framework without the energy index, i.e., time optimal framework; (2) The proposed framework without the path length index, i.e., energy optimal framework. Other parameters of the comparative items are identical to those of the proposed framework. The simulation parameters are shown in Table 1. The planned paths are shown in Fig. 7. The energy storage situation is shown in Fig. 8. The specific results are shown in Table 2.

From the results, on the one hand, though the mission completion time of the time optimal framework is the shortest, the condition that the total energy in the flight process is less than zero appears without taking consideration of the energy index, which is unacceptable for SUAV. On the other hand, the energy optimal framework can make SUAV store the most energy, but the consumed time is also the longest. Compared with the above comparative items, the proposed framework comprehensively considers

**Table 3**  
The fitness statistical results.

| Algorithm | Best   | Worst  | Mean   |
|-----------|--------|--------|--------|
| IWOA      | 213.27 | 216.36 | 214.24 |
| WOA       | 215.21 | 220.05 | 215.98 |
| GWO       | 214.94 | 221.9  | 216.63 |
| GSA       | 216.42 | 225.52 | 219.32 |
| PSO       | 221.41 | 234.59 | 226.01 |

both the time index and the energy index, and realizes the balance of the mission time sensitivity and flight endurance. In the real applications, the weights of the indexes in the proposed framework can be adjusted according to the mission requirements.

### 6.2. Testing the performance of IWOA

The solving performance of IWOA is tested in this section. WOA, GWO, GSA, PSO are selected as comparative solvers. For the fairness of the simulation, the population sizes and the maximum iterations of the comparative solvers are the same as those of IWOA in Table 1. The other parameters of the basic WOA are identical to those of IWOA. The other parameters in the path planning framework are identical to the proposed one except for the solvers. 20 groups of comparative tests are made. A group of typical fitness curves are shown in Fig. 9. The fitness statistical results are shown in Table 3.

From the results, not only the best fitness but also the mean fitness of IWOA are optimal in several typical IOAs. The proposed improvement measures can make WOA effectively avoid the local minima and obtain a higher solving accuracy and faster convergence speed.

## 7. Conclusion

This paper proposes a novel path planning framework for SUAV in urban environment. Aiming at the complex urban environment, three main contributions are made in this paper. First, for the SUAV solar energy production modeling, this paper describes some unreasonable aspects of the previous studies and modifies the model by introducing ASHRAE Clear Sky Model. Meanwhile, for a more precise energy modeling in city, the sunlight occlusions by high buildings are taken into consideration in this paper. Second, for the obstacle avoidance in city, RIFDS is proposed to overcome the defect of divorcing from the dynamic model in the traditional IFDS and provides the necessary angles for the calculation of the energy model. Third, to provide an effective solver for the path planning framework, some improvements are introduced to WOA, and the proposed IWOA is selected as the solver. The proposed IWOA shows a higher solving accuracy and a faster convergence speed, and can effectively avoid the local minima. These three contributions can be closely combined for the application of SUAV in urban environment. In the future, we will focus on two aspects of the related work: First, we will further design the SUAV 3D path planning framework which is more complicated than the proposed 2D framework, and on the basis of 3D planning, we will consider the influences of other environment factors for SUAV in city such as the airflow between buildings. Second, we will further improve our proposed IWOA in the following aspects: (1) The analysis for the computational complexity and convergence of IWOA will be explored; (2) The parallel computing method will be introduced to our IWOA in an attempt to accelerate its computation speed; (3) The performance of the multi-objective IWOA will be explored.

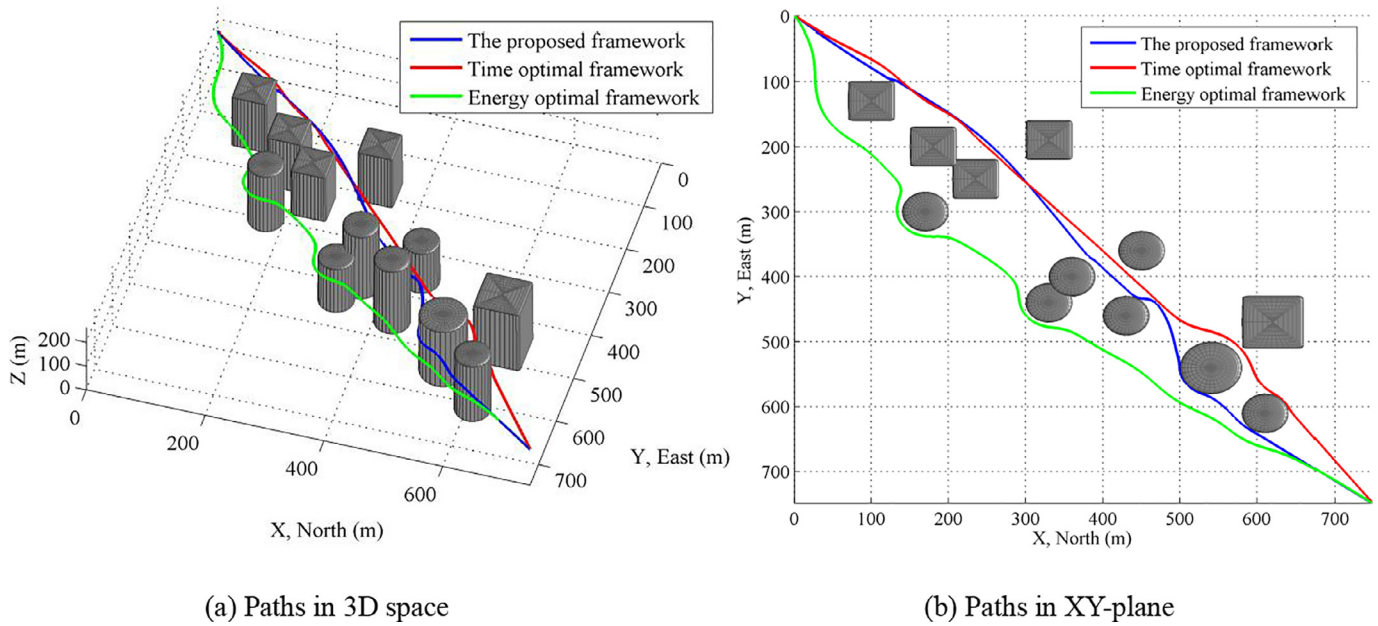


Fig. 7. The planned paths.

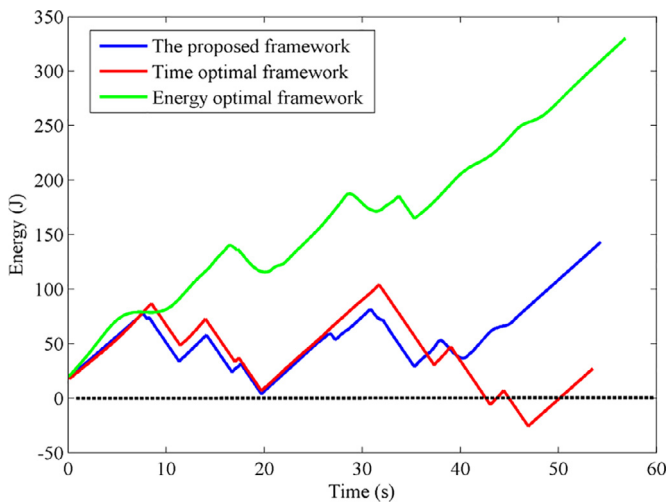


Fig. 8. The energy storage situation.

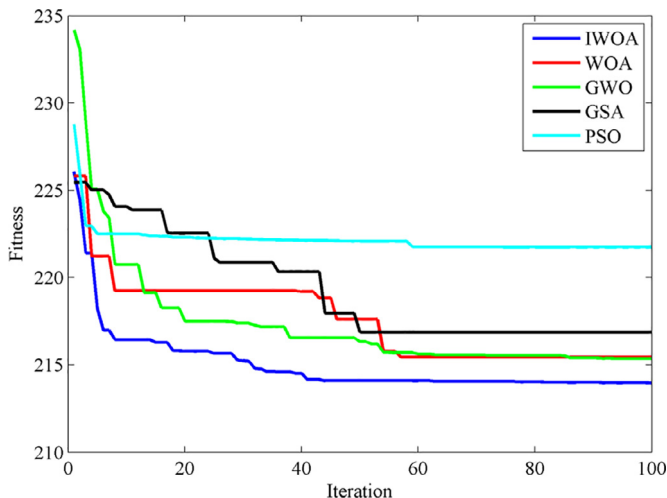


Fig. 9. A group of typical fitness curves with different optimization algorithms.

**Acknowledgments**

This research has been funded in part by the National Natural Science Foundations of China under Grants 61175084, 61673042, in part by Program for Changjiang Scholars and Innovative Research Team in University under Grant IRT 13004. The authors would also like to thank the reviewers and the editor for their comments and suggestions that helped to improve the paper significantly.

**References**

- [1] A.T. Klesh, P.T. Kabamba, Solar-powered aircraft: energy-optimal path planning and perpetual endurance, *J. Guid. Control Dyn.* 32 (4) (2009) 1320–1329.
- [2] S.C. Spangelo, E.G. Gilbert, Power optimization of solar-powered aircraft with specified closed ground tracks, *J. Aircraft* 50 (1) (2012) 232–238.
- [3] X. Gao, Z. Hou, Z. Guo, et al., Energy management strategy for solar-powered high-altitude long-endurance aircraft, *Energy Convers. Manage* 70 (2013) 20–30.
- [4] X. Gao, Z. Hou, Z. Guo, et al., Reviews of methods to extract and store energy for solar-powered aircraft, *Renewable Sustainable Energy Rev* 44 (2015) 96–108.
- [5] X. Zhu, Z. Guo, Z. Hou, Solar-powered airplanes: a historical perspective and future challenges, *Prog. Aerosp. Sci.* 71 (2014) 36–53.
- [6] R. Dai, U. Lee, S. Hosseini, et al., Optimal path planning for solar-powered UAVs based on unit quaternions, in: *Fifty-First IEEE Conference on Decision and Control*, 2012, pp. 3104–3109.
- [7] R. Dai, Path planning of solar-powered Unmanned Aerial Vehicles at low altitude, in: *Fifty-Sixth IEEE International Midwest Symposium on Circuits and Systems*, 2013, pp. 693–696.
- [8] S. Hosseini, R. Dai, M. Mesbahi, Optimal path planning and power allocation for a long endurance solar-powered UAV, in: *Proceeding of 2013 American Control Conference*, 2013, pp. 2588–2593.
- [9] S. Hosseini, M. Mesbahi, Energy-aware aerial surveillance for a long-endurance solar-powered Unmanned Aerial Vehicles, *J. Guid. Control Dyn* 39 (9) (2016) 1980–1993.
- [10] D.Y. Goswami, *Principles of Solar Engineering*, third ed., CRC Press, 2015.
- [11] ASHRAE, *ASHRAE Handbook: Fundamentals (IP & SI)*, ASHRAE, 2013.
- [12] P. Yao, H. Wang, Z. Su, UAV feasible path planning based on disturbed fluid and trajectory propagation, *Chin. J. Aeronaut* 28 (4) (2015) 1163–1177.
- [13] P. Yao, H. Wang, Z. Su, Real-time path planning of unmanned aerial vehicle for target tracking and obstacle avoidance in complex dynamic environment, *Aerosp. Sci. Technol.* 47 (2015) 269–279.
- [14] P. Yao, H. Wang, Z. Su, Cooperative path planning with applications to target tracking and obstacle avoidance for multi-UAVs, *Aerosp. Sci. Technol* 54 (2016) 10–22.
- [15] P. Yao, H. Wang, Dynamic adaptive Ant Lion Optimizer applied to route planning for unmanned aerial vehicle, *Soft. Comput* (2016) 1–14, doi:10.1007/s00500-016-2138-6.

- [16] B. Zhang, H. Duan, Three-dimensional path planning for uninhabited combat aerial vehicle based on predator-prey pigeon-inspired optimization in dynamic environment, *IEEE/ACM Trans. Comput. Biol.* 14 (1) (2017) 97–107.
- [17] P. Li, H. Duan, Path planning of unmanned aerial vehicle based on improved gravitational search algorithm, *Sci. Chin. Technol. Sci.* 55 (10) (2012) 2712–2719.
- [18] C. Xu, H. Duan, F. Liu, Chaotic artificial bee colony approach to Uninhabited Combat Air Vehicle (UCAV) path planning, *Aerosp. Sci. Technol.* 14 (8) (2010) 535–541.
- [19] Y. Chen, J. Yu, Y. Mei, et al., Modified central force optimization (MCFO) algorithm for 3D UAV path planning, *Neurocomputing* 171 (2016) 878–888.
- [20] H. Qu, K. Xing, T. Alexander, An improved genetic algorithm with co-evolutionary strategy for global path planning of multiple mobile robots, *Neurocomputing* 120 (2013) 509–517.
- [21] P.K. Das, H.S. Behera, S. Das, et al., A hybrid improved PSO-DV algorithm for multi-robot path planning in a clutter environment, *Neurocomputing* 207 (2016) 735–753.
- [22] Z. Sun, J. Wu, J. Yang, et al., Path planning for GEO-UAV bistatic SAR using constrained adaptive multiobjective differential evolution, *IEEE Trans. Geosci. Remote Sens.* 54 (11) (2016) 6444–6457.
- [23] Z. Su, H. Wang, A novel robust hybrid gravitational search algorithm for reusable launch vehicle approach and landing trajectory optimization, *Neurocomputing* 162 (2015) 116–127.
- [24] S. Mirjalili, S.M. Mirjalili, A. Lewis, Grey wolf optimizer, *Adv. Eng. Softw.* 69 (2014) 46–61.
- [25] Z. Su, H. Wang, P. Yao, A hybrid backtracking search optimization algorithm for nonlinear optimal control problems with complex dynamic constraints, *Neurocomputing* 186 (2016) 182–194.
- [26] S. Mirjalili, A. Lewis, The Whale Optimization Algorithm, *Adv. Eng. Softw.* 95 (2016) 51–67.
- [27] J. Wu, H. Wang, N. Li, et al., Distributed trajectory optimization for multiple solar-powered UAVs target tracking in urban environment by Adaptive Grasshopper optimization algorithm, *Aerosp. Sci. Technol.* 70 (2017) 497–510.
- [28] S. Freitas, C. Catita, P. Redweik, et al., Modelling solar potential in the urban environment: State-of-the-art review, *Renewable Sustainable Energy Rev.* 41 (2015) 915–931.
- [29] R. Erdélyi, Y.M. Wang, W.S. Guo, et al., Three-dimensional Solar Radiation Model (SORAM) and its application to 3-D urban planning, *Sol. Energy* 101 (2014) 63–73.
- [30] T. Bai, Y. Kan, J. Chang, et al., Fusing feasible search space into PSO for multi-objective cascade reservoir optimization, *Appl. Softw. Comput.* 51 (2017) 328–340.
- [31] H. Mokhtari, A. Salmasnia, A Monte Carlo simulation based chaotic differential evolution algorithm for scheduling a stochastic parallel processor system, *Expert Syst. Appl.* 42 (20) (2015) 7132–7147.
- [32] S. Mirjalili, A.H. Gandomi, Chaotic gravitational constants for the gravitational search algorithm, *Appl. Soft. Comput.* 53 (2017) 407–419.
- [33] Y. Wei, J. Qiu, S. Fu, Mode-dependent nonrational output feedback control for continuous-time semi-Markovian jump systems with time-varying delay, *Nonlinear Anal.: Hybrid Syst.* 16 (2015) 52–71.
- [34] Y. Wei, J. Qiu, H.K. Karimi, Quantized  $\mathcal{H}_\infty$  filtering for continuous-time Markovian jump systems with deficient mode information, *Asian. J. Control* 17 (5) (2015) 1914–1923.
- [35] T. Back, *Evolutionary Algorithms in Theory and Practice: Evolution Strategies, Evolutionary Programming, Genetic Algorithms*, Oxford University Press, 1996.



**Jianfa Wu** was born in Hebei, China, in 1993. He received the B.S. degree in Automation from Harbin Engineering University, China. He is currently a Ph.D. candidate in Navigation, Guidance and Control, School of Automation Science and Electrical Engineering, Beihang University (BUAA). His current research interests include cooperative control and path planning of multi-agents, autonomous decision and control of solar-powered UAV.



**Honglun Wang** was born in Shaanxi, China, in 1970. He received the B.S., M.S., and Ph.D. in Fire Control from Northwestern Polytechnical University, China, in 1992, 1995 and 1998. He did postdoctoral research at Nanjing University of Aeronautics and Astronautics, China. In 2000, Beihang University (BUAA), as a professor affiliated with Navigation, Guidance and Control. He was chosen by the New Century Excellent Researcher Award Program from Ministry of Education of China in 2009. His research interests include autonomous flight control for UAVs, sense and avoid technology for UAVs, theory and method of path planning in complex environments for UAVs.



**Na Li** was born in Shaanxi, China, in 1970. She received the B.S. degree from Xi'an Jiaotong University, China, and the M.S. degree in Precision Instrument and Machinery from Beihang University (BUAA), China, in 1993 and 2006, respectively. She is currently an associate professor with Unmanned System Research Institute, Beihang University. Her current research interests include autonomous flight control for UAVs, software engineering.



**Peng Yao** was born in Shandong, China, in 1989. He received the B.S. degree in Automation from Shandong University, China, and the Ph.D. degree in Navigation, Guidance and Control from Beihang University (BUAA), China, in 2011 and 2017, respectively. He is currently a lecturer with the College of Engineering, Ocean University of China. His current research interests include intelligent decision and path planning of unmanned vehicle, cooperative optimization and control of multi-agents.



**Yu Huang** was born in Hunan, China, in June 1989. He received the B.S. degree in Automation from Xi'an University of Posts & Telecommunications, China, the M.S. degree in Pattern Recognition and Intelligent System from Shenyang Aerospace University, China, and the Ph.D. degree in Navigation, Guidance and Control from Beihang University (BUAA), China, in 2007, 2010 and 2017, respectively. He is currently doing postdoctoral research at Tsinghua University, China. His current research interests include autonomous decision and control of solar-powered UAV.



**Hemeng Yang** received the Ph.D. degree in Optical Engineering from Tianjin University, China, in 2012. He subsequently joined China Academy of Space Technology (CAST) as a senior engineer. His current research interests include aerial remote sensing technique, unmanned aircraft system integration design.